Minerals **2014**, *4*, 170-190; doi:10.3390/min4010170

OPEN ACCESS

minerals

ISSN 2075-163X
www.mdpi.com/journal/minerals

Article

Acidic Microenvironments in Waste Rock Characterized by Neutral Drainage: Bacteria–Mineral Interactions at Sulfide Surfaces

John W. Dockrey [1,†], Matthew B. J. Lindsay [2], K. Ulrich Mayer [1,*], Roger D. Beckie [1], Kelsey L. I. Norlund [3,‡], Lesley A. Warren [3] and Gordon Southam [4]

[1] Department of Earth, Ocean and Atmospheric Sciences, The University of British Columbia, 2207 Main Mall, Vancouver, BC V6T 1Z4, Canada; E-Mail: rbeckie@eos.ubc.ca

[2] Department of Geological Sciences, University of Saskatchewan, Saskatoon, SK S7N 5E2, Canada; E-Mail: matt.lindsay@usask.ca

[3] School of Geography and Earth Sciences, McMaster University, Hamilton, ON L8S 4L8, Canada; E-Mail: warrenl@mcmaster.ca

[4] School of Earth Sciences, The University of Queensland, St. Lucia, QLD 4072, Australia; E-Mail: g.southam@uq.edu.au

† Present Address: Lorax Environmental Services Ltd., Vancouver, BC V6J 3H9, Canada; E-Mail: jdockrey@lorax.ca

‡ Present Address: Rescan Environmental Services Ltd., Vancouver, BC V6E 2J3, Canada; E-Mail: kelsey.norlund@gmail.com

* Author to whom correspondence should be addressed; E-Mail: umayer@eos.ubc.ca; Tel.: +1-604-822-1539; Fax: +1-604-822-6088.

Received: 13 January 2014; in revised form: 4 March 2014 / Accepted: 17 March 2014 / Published: 21 March 2014

Abstract: Microbial populations and microbe-mineral interactions were examined in waste rock characterized by neutral rock drainage (NRD). Samples of three primary sulfide-bearing waste rock types (*i.e.*, marble-hornfels, intrusive, exoskarn) were collected from field-scale experiments at the Antamina Cu–Zn–Mo mine, Peru. Microbial communities within all samples were dominated by neutrophilic thiosulfate oxidizing bacteria. However, acidophilic iron and sulfur oxidizers were present within intrusive waste rock characterized by bulk circumneutral pH drainage. The extensive development of microbially colonized porous Fe(III) (oxy)hydroxide and Fe(III) (oxy)hydroxysulfate precipitates was observed at

sulfide-mineral surfaces during examination by field emission-scanning electron microscopy-energy dispersive X-ray spectroscopy (FE-SEM-EDS). Linear combination fitting of bulk extended X-ray absorption fine structure (EXAFS) spectra for these precipitates indicated they were composed of schwertmannite [$Fe_8O_8(OH)_{6-4.5}(SO_4)_{1-1.75}$], lepidocrocite [γ-FeO(OH)] and K-jarosite [$KFe_3(OH)_6(SO_4)_2$]. The presence of schwertmannite and K-jarosite is indicative of the development of localized acidic microenvironments at sulfide-mineral surfaces. Extensive bacterial colonization of this porous layer and pitting of underlying sulfide-mineral surfaces suggests that acidic microenvironments can play an important role in sulfide-mineral oxidation under bulk circumneutral pH conditions. These findings have important implications for water quality management in NRD settings.

Keywords: mine tailings; neutral rock drainage; biooxidation; Fe- and S-oxidizing bacteria; synchrotron; EXAFS

1. Introduction

The extraction and processing of ore deposits generate immense quantities of mine wastes. Waste rock and mill tailings generated at mines exploiting sulfide ore deposits, which are a primary source of base and precious metals, pose a substantial risk to water quality. Mine wastes commonly are deposited under atmospheric conditions where sulfide minerals, for example pyrite [FeS_2] or pyrrhotite [$Fe_{1-x}S$], become thermodynamically unstable [1]. Oxidative dissolution of these and other sulfide minerals generates acidity, and releases sulfate, iron and associated metals to pore waters. The quality of drainage emanating from sulfide-bearing mine wastes is dependent on many factors, including mineralogical and geochemical properties, hydrogeologic conditions, and the activity of lithoautotrophic microorganisms [2]. Despite ongoing sulfide-mineral oxidation, neutral rock drainage (NRD) conditions may persist in mine wastes containing an abundance of carbonate minerals [3]. Principal threats to water quality under circumneutral pH conditions are weakly-hydrolyzing metals, including Zn, Ni, Cu(I) and Fe(II), and oxyanion-forming metals, including Mo, As, Se and Cr [4,5]. Exhaustion of the intrinsic acid-neutralization capacity of waste rock or mill tailings may facilitate generation of acidic rock drainage (ARD) and large increases in dissolved concentrations of Zn, Ni, Cu, Fe and other metals [6,7].

Mechanisms of sulfide-mineral oxidation in ARD settings are well established. Under acidic pH conditions, chemical oxidation by Fe(III) is the predominant oxidation mechanism and microbially-catalyzed Fe(II) oxidation largely controls overall reaction rates [8–10]. The importance of this oxidation mechanism could be expected to diminish at circumneutral pH due to limitations on Fe(III) solubility. Nevertheless, acidophilic iron oxidizing bacteria (e.g., *Acidithiobacillus ferrooxidans*) and acidophilic sulfur oxidizing bacteria (e.g., *Acidithiobacillus thiooxidans*) have been cultured from NRD settings, where a pH limitation on growth would be anticipated [5,11–13]. Although acidophiles may be active within NRD systems, associated microbial communities are commonly dominated by neutrophilic sulfur oxidizing bacteria (*i.e.*, *Thiobacillus* spp.) [5,12,13]. These bacteria mediate the

oxidation of intermediate sulfur compounds, including thiosulfate ($S_2O_3^{2-}$), trithionate ($S_3O_6^{2-}$) and tetrathionate ($S_4O_6^{2-}$), which form as a result of sulfide-mineral oxidation by Fe(III) at circumneutral pH [14–16]. At acidic pH, elemental sulfur (S_8^0), pentathionate ($S_5O_6^{2-}$) and sulfate (SO_4^{2-}) are important products of Fe(III) oxidation of sulfide minerals [16]. In these environments, sulfur oxidizing bacteria are thought to enhance oxidation rates by limiting the accumulation of reaction products or inhibiting the formation of secondary sulfur-bearing precipitates at sulfide-mineral surfaces [17].

The degree to which acidophilic iron oxidizers catalyze sulfide-mineral oxidation under bulk circumneutral pH conditions remains poorly constrained. The importance of Fe(III) oxidation of sulfides within NRD settings is dependent on the solubility of Fe(III) and activity of acidophilic iron oxidizing bacteria at the sulfide-mineral surface. Southam and Beveridge [11] proposed that acidophilic iron oxidizers overcome pH limiting growth conditions by forming acidic microenvironments at sulfide-mineral surfaces. This hypothesis was subsequently confirmed through detailed microscopy studies, which revealed close association of *A. ferrooxidans* to sulfide-mineral surfaces and the corresponding occurrence of Fe(III) (oxy)hydroxide and Fe(III) (oxy)hydroxysulfate minerals [18,19]. These secondary Fe(III) phases generally are thought to enhance the Fe(III) solubility within close proximity of the mineral surface, and limit diffusive transport of sulfide-oxidation products to bulk solution [18]. Extracellular polymeric substances (EPS) deposited by acidophilic bacteria also may contribute to enhanced dissolution rates by complexing Fe(III) compounds, thereby making them available for sulfide-mineral oxidation [20]. Ongoing development of acidic microenvironments due to bacterial growth, EPS deposition and mineral precipitation at the sulfide-mineral surface may have important implications for sulfide-mineral oxidation within NRD settings. Understanding mechanisms of sulfide mineral-oxidation and metal transport in NRD settings, and anticipating temporal or spatial transitions between NRD and ARD conditions, is central to the development and implementation of effective strategies for water quality management at mining operations.

The objective of this study was to examine the role of acidophilic bacteria within waste rock characterized by bulk circumneutral pH conditions. Additionally, this study aimed to assess mechanisms by which acidophiles colonize sulfide-mineral surfaces under these conditions. Samples of sulfide-bearing waste rock were collected from field-scale experiments conducted at the Antamina Cu–Zn–Mo mine, Peru. Culture-dependent and culture-independent techniques were used to examine the distribution of neutrophilic and acidophilic bacteria. Fluorescence *in situ* hybridization (FISH) was employed to probe the presence of *Acidithiobacillus* spp. within the samples. Secondary electron scanning electron microscopy (SEM)-equipped with Energy Dispersive Spectroscopy (EDS), powder X-ray diffraction (XRD) and X-ray absorption spectroscopy (XAS) were utilized to examine microbial-mineral interactions at surfaces of sulfide minerals.

2. Experimental Section

2.1. Site Description

The Antamina Cu–Zn–Mo mine is located in the Peruvian Andes (9°32' S, 77°03' W), approximately 270 km northeast of Lima, at an elevation of 4300 m above sea level. Despite its high elevation, mean annual temperatures ranged from 5.4 to 8.5 °C between 2001 and 2009, which is reflective of the

tropical latitude of the mine. Approximately 80% of the average annual rainfall of ~1200 mm occurs during the wet season, which typically lasts from November to April. The mine exploits a Cu–Zn skarn deposit with ore-grade mineralization transported via quartz-monzonite porphyries intruding Cretaceous limestone strata. For a detailed description of the lithologic, stratigraphic, and structural setting of Antamina, see Love and Clark [21]. Pyrite and chalcopyrite [$CuFeS_2$] are the dominant sulfide minerals within the orebody, while molybdenite [MoS_2], sphalerite [(Zn,Fe)S], pyrrhotite and arsenopyrite [FeAsS] are less abundant. Waste rock from the open pit is stored in large, unsaturated piles that extend vertically by >400 m. Acidity generated by sulfide-mineral oxidation is largely neutralized by carbonate minerals, which are abundant within the waste rock. Bulk drainage from the waste rock piles is generally characterized by circumneutral pH conditions and discharge concentrations of Zn, As, Se and Mo are the water quality parameters of principal concern at the mine.

Three large-scale experimental waste rock piles were constructed for this project by the Antamina mine for use between 2006 and 2009; approximately three years of weathering. A primary objective of this experiment was to characterize drainage quality from waste rock composed of three primary lithologic units associated with the ore body (Table 1). These experimental piles each were constructed using 25–30 kt of waste rock, which was deposited by end-dumping from a 10 m high access ramp onto a 36 m × 36 m basal lysimeter constructed of impermeable geotextile liner. Instrumentation to facilitate monitoring of spatial and temporal variations in hydrology and geochemistry was installed within each experimental waste rock pile. Additionally, a series of complementary field-scale weathering (bioleaching) experiments was initiated to monitor geochemical evolution of drainage from the individual rock types included in the experimental waste rock piles (Table 1). These field-cell experiments were established as lysimeters containing 260–350 kg of waste rock overlying 15 cm of silica sand within 208 L (*i.e.*, 55 U.S. liquid gallons) high-density polyethylene drums. The tops of the lysimeters were open to the atmosphere to facilitate infiltration, gas transport, and microbial colonization via wind-blown particles.

Table 1. Summary of average drainage pH and calculated cumulative mass discharges for July 2008–June 2009. Weathering duration indicates number of years since initiating the experiment. Parameters with values < 0.1 $mg \cdot kg^{-1}$ were not reported.

Lithologic Unit	Experimental ID	Weathering Duration (year)	pH_{avg}	Cumulative mass discharge ($mg \cdot kg^{-1}$)			
				SO_4^{2-}	Zn	Mo	Cu
Marble-hornfels	Pile 1	2.5	7.73	35			
Intrusive	FC-1-3A	2.6	7.85	140	2.6		0.1
	Pile 2	1.5	7.45	78	0.5	0.3	
	FC-2-2B	1.5	7.88	170	0.3	7.1	
Exoskarn	FC-2-3A	1.4	6.18	310	17		13
	Pile 3	1.5	7.46	100	1.5		
	FC-3-2A	1.4	7.32	590	15		0.1

2.2. Sample Collection and Preservation

Samples of marble-hornfels (Pile 1, FC1-3A), intrusive (Pile 2, FC-2-2B, FC2-3A) and exoskarn (Pile 3, FC-3-2A) waste rock types were collected in February 2009, at the height of the rainy season.

These samples were selected because they represent the three primary waste rock lithologies at the study site. For comparison, separate samples for each waste rock type were collected from the experimental piles and from the field cells. Samples from the field cells were extracted from holes cut immediately above the interface between the waste rock and underlying silica sand. For the experimental piles, samples were collected from the base of 1 m deep test pits excavated at the top central region of each pile. Bulk samples ranging in mass from 200 to 250 g were placed in 200 mL polyethylene bottles (Nalgene, Rochester, NY, USA). Sub-samples of metal sulfides from these sample bottles, selected for field emission-scanning electron microscopy (FE-SEM) imaging, were rinsed three times with deionized water and field fixed with 1% (*v*/*v*) glutaraldehyde (Electron Microscopy Sciences, Hatfield, PA, USA) in sterile 50 mL polypropylene conical centrifuge tubes (Falcon; BD Biosciences, San Jose, CA, USA). All samples were shipped to the University of British Columbia for analysis. Additional mineral grains, selected for FE-SEM imaging from the bulk samples, were fixed with 1% (*v*/*v*) glutaraldehyde in the laboratory.

2.3. Mineralogical and Geochemical Analyses

Quantitative mineralogical analysis was performed by powder XRD and Rietveld refinement. A mortar and pestle was used to crush 40 to 50 g sub-samples of material from each location to <1 mm, and further grinding to <5 μm utilized a micronizing mill (McCrone Microscopes and Accessories, Westmont, IL, USA). The powdered samples were then mounted as pressed pellets, and XRD patterns were collected by step scanning from 3°–80° 2θ using a CuKα X-ray source supplied by a Siemens D5000 Bragg-Brentano diffractometer (Siemens AG, Munich, Germany). The scan data was refined using the Rietveld analysis program Topas 3.0 (Coelho Software, Brisbane, Australia). Subsequent examination using a Philips XL30 (FEI™, Hillsboro, OR, USA) scanning electron microscope (SEM) equipped with a Bruker Quanta 200 (Milton, ON, Canada) energy-dispersion X-ray microanalysis system (EDS) to assess the presence of geochemically important minerals (*i.e.*, sulfides, carbonates and phosphates) not detected by powder XRD. Fine-grained samples were mounted on aluminum stubs using carbon tape, and sputter coated with carbon to ensure conductance. An accelerating potential of 15 kV was used for imaging and semi-quantitative chemical analyses.

The local atomic environment of Fe in secondary mineral phases was examined by synchrotron- based X-ray absorption spectroscopy (XAS). Extended X-ray adsorption fine structure (EXAFS) spectra for Fe were collected on beamline 11-2 at the Stanford Synchrotron Radiation Lightsource (Menlo Park, CA, USA). A double crystal Si(220) monochromator was utilized for energy selection and scans were conducted from +100 to +1000 eV relative to the Fe K-edge (E_0 = 7111 eV). The data reduction software SIXPACK/IFEFFIT was used to isolate backscattering contributions by subtracting a spline function from the EXAFS data region [22]. The results were then converted from eV to k($Å^{-1}$) and weighted by k^3 and windowed from 3 to 14 $Å^{-1}$. Least squares linear combination fitting (LCF) was performed to assess the occurrence of Fe(III) (oxy)hydroxide and Fe(III) (oxy)hydroxysulfate phases.

Solid-phase concentrations of metals were determined by X-ray fluorescence (XRF) spectroscopy (PW-2400; PANalytical B.V., Almelo The Netherlands), whereas sulfur and carbon contents were quantified using combustion-infrared absorption (CNS-1000; LECO Corp., St. Joseph, MI, USA). Sample fractions that passed through a 1.18 mm sieve were ground and pulverized using methods

similar to those described for XRD analysis. This size fraction was selected for elemental analysis because silt-sized and clay-sized particles generally comprise the majority of reactive surface area within mine waste deposits [23]. Fusion pellets for major oxide analyses were prepared using Li-tetraborate/Li-metaborate, whereas trace element concentrations were determined for samples prepared as pressed powder pellets.

2.4. Microbial Enumerations

Due to the coarse texture and variability in grain-size distribution among samples, microbial characterization focused on the fine-grained (*i.e.*, sub-millimeter) fraction separated from the samples by a DI water wash. This wash was performed by adding 40 mL of sterile DI water to the 200 mL sample bottles containing 200–250 g of waste rock. The bottles were sealed, shaken vigorously by hand, 30 times through the arc of 50 cm and the suspended sediment was decanted into sterile 50 mL Falcon tubes. Isolated particles were suspended in solution by manual shaking and then vortex mixing for 30 s prior to analysis. Dry weights of solids in this suspension were determined for mass normalization among samples.

Culture-dependent and culture-independent techniques were used to characterize the microbial community. A five-tube most probable number (MPN) approach was used to enumerate iron-oxidizing acidophiles, sulfur-oxidizing acidophiles and thiosulfate-oxidizing neutrophiles [24]. The culture medium for iron oxidizers was comprised of a basal salt solution and an Fe(II) stock solution, which were prepared separately to prevent Fe(II) oxidation prior to inoculation. The basal salt solution was prepared by dissolving (0.9 L^{-1}) 0.4 g $(NH_4)_2SO_4$, 0.1 g K_2HPO_4 and 0.4 g $MgSO_4 \cdot 7H_2O$ in DI water, and adjusting the pH to 2.2 using H_2SO_4. The Fe(II) stock was prepared by dissolving (L^{-1}) 33.3 g $FeSO_4 \cdot 7H_2O$ into DI water that had previously been acidified to pH 2.2 with H_2SO_4. These solutions were filter sterilized through 0.45 μm membranes, and 4.5 mL of stock solution plus 0.5 mL of Fe(II) stock solution were combined in sterile culture tubes.

Sulfur-oxidizing acidophiles were grown in a culture medium prepared by dissolving (L^{-1}) 0.3 g $(NH_4)_2SO_4$, 0.1 g KH_2PO_4, 0.4 g $MgSO_4 \cdot 7H_2O$, 0.33 g $CaCl_2 \cdot 2H_2O$ and 18 mg $FeSO_4 \cdot 7H_2O$ in DI water and adjusting the final pH to 2.3 using H_2SO_4. The culture medium for thiosulfate oxidizing neutrophiles was prepared by adding (L^{-1}) 0.3 g $(NH_4)_2SO_4$, 0.1 g KH_2PO_4, 0.4 g $MgSO_4 \cdot 7H_2O$, 0.33 g $CaCl_2 \cdot 2H_2O$ and 4.93 g $Na_2S_2O_3 \cdot 5H_2O$ to DI water and adjusting the final pH to 7 with NaOH. These media were filter sterilized through a 0.45 μm membrane, and 5 mL aliquots were dispensed into separate sterile culture tubes. Inoculation was performed by pipetting 1 mL of the sample suspension into each of five sterile culture tubes containing a given culture medium. A series of nine 10-fold serial dilutions was performed immediately following inoculation, and the contents of each tube were vortexed for 30 s prior to each dilution. Following inoculation, a thin film of ~0.15 g of elemental (sublimed) S was added as a substrate for the sulfur-oxidizing acidophiles. Results for all MPN enumerations were tabulated after a six-week incubation period at room temperature (~21 °C).

Total (live and dead) bacteria were quantified using a Live/Dead® Baclight™ bacterial viability kit (Molecular Probes Inc., Burlington, ON, Canada). This fluorescence-based assay distinguishes between live and dead cells using two nucleic acid stains: (1) a green fluorescent stain, SYTO® 9, which labels membranes of both live and dead cells; and (2) a red fluorescent stain, propidium iodide,

which selectively labels only damaged (dead) cell membranes. Propidium iodide preferentially labels dead cells over SYTO® 9; therefore, bacterial viability can be assessed through quantification of both live and dead cells. The assays were initiated by pipetting 6 µL of sample suspension into 1 mL of sterile DI water contained in micro-centrifuge tubes. The addition of 3 µL of a 1:1 (*v*/*v*) mixture of each stain preceded incubation in the dark and at room temperature. After 15 min, the solution was passed through a 0.1-µm filter and retained bacterial cells were counted by fluorescence photomicroscopy (Nikon Optiphot-2, Melville, NY, USA). The integrated criteria of shape, size, and fluorescence were used to distinguish stained bacteria from autofluorescence and non-specific binding of fluorophores to clay particles.

2.5. Fluorescence in Situ Hybridization

Fluorescence *in situ* hybridization (FISH) uses fluorescently tagged oligonucleotide probes to identify specific rRNA sequences within microbial cells. Probes specific to different taxonomic levels, including at the genus and species levels, have been developed and can be applied to whole-cell hybridization of environmental and laboratory samples providing valuable insight into microbial community structure, spatial arrangement and cell viability [25].

Samples of fines (as above) were suspended in 3 mL PBS solution (L^{-1} distilled water: 8 g NaCl, 0.2 g KCl, 1.44 g Na_2HPO_4 and 0.24 g KH_2PO_4, pH-adjusted to 7.4) and preserved in 4% paraformaldehyde for 16 h. Gelatin-coated slides (ethanol-sterilized slides coated by dipping in a 50 °C filter-sterilized solution of 0.1% (*w*/*v*) gelatin and 0.01% (*w*/*v*) $KCr(SO_4)_2$ prepared in distilled water) were UV-irradiated for 30 min. Five µL of sample was applied to the slide, smearing it with the end of the pipette tip in a dime-sized circle. Slides were air-dried in a sterile environment for 1 h at room temperature. Samples were dehydrated by soaking slides in an increasing ethanol series (3 min at 50%, 80% and 95% ethanol) and air-dried in a sterile environment for 1 h at room temperature. Twenty-five microliter of hybridization solution (24 µL of hybridization buffer (0.9 M NaCl, 100 mM Tris, 1% SDS and 20% formamide) and 50 ng of probe) was applied to the dried sample. Samples were covered with plastic cover slips to ensure even hybridization. The probe used was the genus-specific molecular probe Thio820 (ACCAAACATCTAGTATTCATC 5′-labelled Alexafluor 647; *Acidithiobacillus*). Slides were incubated in the dark at 37 °C for 4–9 h in a container kept humid by tissues soaked in hybridization buffer. Cover slips were removed following hybridization by dipping slides into staining jars filled with hybridization buffer equilibrated to 37 °C. Slides were rinsed twice (10 min shaking in a water bath) in a wash buffer (0.5 M NaCl, 100 mM Tris, 5 mM EDTA, 0.1% SDS) equilibrated to 37 °C followed by a final rinse in distilled water. Slides were then air-dried in the dark at room temperature. Slides were counterstained with 20 µL of DAPI (1 µg/mL) and glass cover slips were sealed over the sample. Fluorescence imaging was performed with a Leica LEITZ DMRX epifluorescence microscope (Leica Microsystems, Richmond Hill, ON, Canada). Openlab 2.2.5 (Improvision, Coventry, UK) was used for digital imaging.

2.6. Electron Microscopy

Two samples of weathered metal sulfides (phenotypic evidence of oxidation) were collected from each of the three experimental waste rock piles (Pile 1, Pile 2 and Pile 3) and one field cell (FC-2-3A)

for detailed examination by electron microscopy. Samples fixed in 1% glutaraldehyde were dehydrated through a graded ethanol series (25, 50, 75 and 100 vol % ethanol for 30 min each) and dried using a SamDri® $CO_{2(l)}$ critical-point drier (Tousimis Research Corp., Rockville, MD, USA) to preserve cell structure. Samples were mounted on aluminum stubs using carbon tape and coated with platinum to ensure conductance.

Imaging and semi-quantitative chemical analysis was performed on a LEO 1540XB field emission-scanning electron microscope (Carl Zeiss SMY AG, Oberkochen, Germany) fitted with an EDAX™ (Ametek, Berwyn, PA, USA) energy dispersive X-ray spectrometer (FE-SEM-EDS). An accelerating potential of 3 kV was used for secondary electron (SE) imaging and EDS spectra were collected at a 10 kV accelerating potential. Cross-sections of sulfide-mineral surfaces were exposed for FE-SEM-EDS examination by sputter milling with an integrated focused ion beam (FIB).

3. Results and Discussion

3.1. Bulk Mineralogy and Geochemistry

Calcite was observed in samples from experiments containing marble-hornfels and exoskarn waste rock (Table 2). The calcite content of the marble-hornfels, which generally occurs at the margins of the deposit, was 67 wt % for FC-1-3A and 53 wt % for Pile 1. Calcite contents for experimental samples containing exoskarn were 9.1 wt % (FC-3-2A) and 3.0 wt % (Pile 3). Calcite was not detected by powder XRD analysis of intrusive rock samples (FC-2-2B, FC-2-3A and Pile 2); however, this acid-neutralizing phase is present in intrusive rocks from the Antamina deposit. The pH of drainage emanating from experimental piles and field cells containing marble-hornfels or exoskarn ranged from 7.3 to 7.9 between July 2008 and June 2009 (Table 1). Calcite was detected as a primary component of the mineral assemblage in these samples, and the observed pH values are indicative of carbonate-mineral dissolution.

Table 2. Results of mineralogical investigation using X-ray diffraction (XRD) and scanning electron microscopy-energy dispersive X-ray spectroscopy (SEM-EDS). Minerals detected by XRD are reported in wt % determined during Rietveld refinement.

Lithologic Unit	Experimental ID	Mineral Abundance (wt %)							
		Cal	Py	Ccp	Sp	Mo	Gn	Apy	Po
Marble-Hornfels	Pile 1	53	0.8		0.7	0.3			
Intrusive	FC-1-3A	67	1.4			*	0.2		
	Pile 2		0.3	0.9		<0.1			
	FC-2-2B		0.5	0.8				*	
Exoskarn	FC-2-3A		1.7	2.6		0.2			*
	Pile 3	3.0	13.0	3.7	1.1				
	FC-3-2A	9.1	8.6	0.9	5.1				

Note: * Mineral phases detected by SEM-EDS and not XRD.

Sulfide minerals were detected in waste rock from all experiments; however, samples of exoskarn consistently exhibited the greatest sulfide-mineral content. Pyrite was the most abundant sulfide mineral in the exoskarn (Pile 3, FC-3-2A) and marble-hornfels (Pile 1, FC-1-3A) rock types, while

chalcopyrite was the most abundant sulfide mineral in the intrusive (Pile 2, FC-2-2B, FC-2-3A) waste rock. In addition to chalcopyrite, samples from experiments that contained intrusive waste rock also contained pyrite (0.3 to 1.7 wt %) and molybdenite (≤0.2 wt %). Subsequent examination of these samples by SEM-EDS confirmed the presence of arsenopyrite (FC-2-2B) and pyrrhotite (FC-2-3A).

The bulk geochemistry of the samples largely reflected the mineral assemblage of the waste rock (Figure 1). Concentrations of Fe, Cu and Zn generally corresponded to the relative abundance of pyrite, chalcopyrite and sphalerite, respectively. Low concentrations of Mo and Pb were detected in samples where molybdenite and galena were not detected by XRD, suggesting these phases were present in low amounts. Furthermore, trace concentrations of As were observed in waste rock samples, which is indicative of the presence of arsenopyrite or other As-bearing minerals at low abundance in these waste rock types. Total-S contents generally corresponded to total sulfide-mineral abundance, whereas elevated total-C concentrations were observed for samples where calcite was identified by XRD. Low total-C concentrations also were detected in samples of intrusive waste rock (Pile 2, FC-2-2B, FC-2-3A) where calcite could not be detected in XRD patterns.

Figure 1. Whole-rock analyses by X-ray fluorescence (XRF) (Fe, Cu, Zn, Mo, Pb and As) or combustion-infrared detection (S and C) for waste rock samples collected in February 2009.

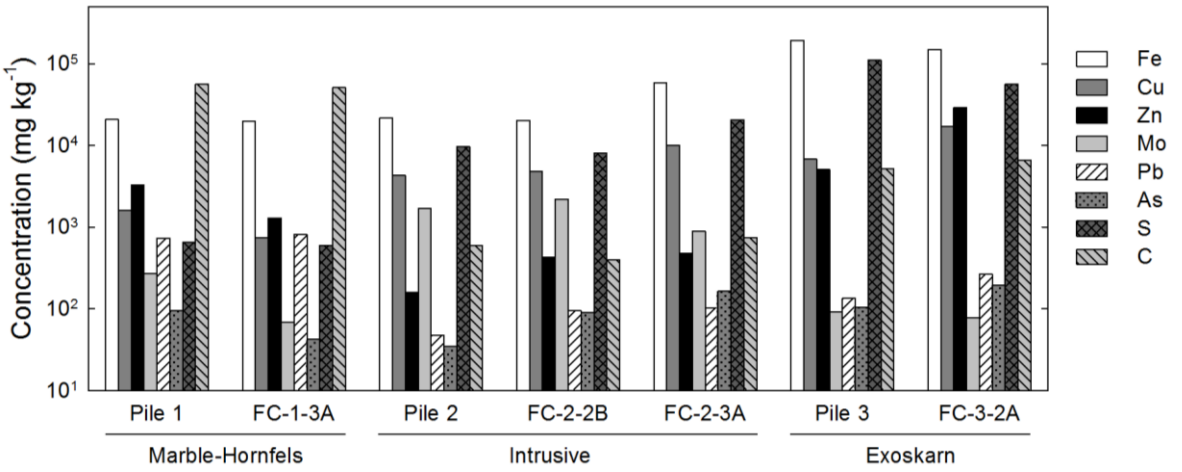

3.2. Microbiology

Populations of neutrophilic thiosulfate oxidizers were clearly abundant in all piles; exceeding a million per gram, with populations ranging from 3.6×10^6 to 2.2×10^8 MPN·g^{-1} of washed sediment (Figure 2). Growth of acidophiles was observed only for samples of intrusive waste rock collected from Pile 2 and FC-2-3A. Elevated populations of acidophilic iron oxidizers (6.5×10^6 MPN·g^{-1}) and sulfur oxidizers (1.1×10^7 MPN·g^{-1}) were associated with the field cell, while only acidophilic iron oxidizers (4.9×10^1 MPN·g^{-1}) were successfully cultured from Pile 2. Cultured acidophiles were capable of oxidizing both Fe and S, which is indicative of *Acidithiobacillus ferrooxidans* as opposed to other commonly-identified acidophiles (e.g., *Acidithiobacillus thiooxidans*, *Leptospirillum ferrooxidans*).

Total bacterial populations estimated from direct counts of live and dead bacteria viability ranged from 1.0×10^7 to 3.4×10^8 bacteria g^{-1} (Figure 2). In five of the seven samples the bacteria were >75% viable, indicating that the microbial populations were likely active within the experimental waste rock

piles and field cells. The two samples with highest populations as measured by both Live/Dead Baclight™ and MPN techniques (Figure 2) also exhibited the lowest proportion of living bacteria (Pile 3, FC-3-2A). This difference may be indicative of geochemical stress resulting from biological activity in the exoskarn waste rock, which exhibited the greatest sulfide-mineral and metal contents, and an average annual pH of 7.4. The total count value can be less than the cultured count when you consider that bacteria occurring "underneath" minerals are not counted; therefore, the microscopic counts are underestimates of the total number of bacteria.

Figure 2. Bacterial enumerations performed on waste rock samples collected in February 2009. Enumerations of total and live bacteria performed using Live/Dead Baclight™. Culture-based enumeration of *Thiobacillus* spp., e.g., *A. thiooxidans* and *A. ferrooxidans*, was performed using the most probable number (MPN) technique.

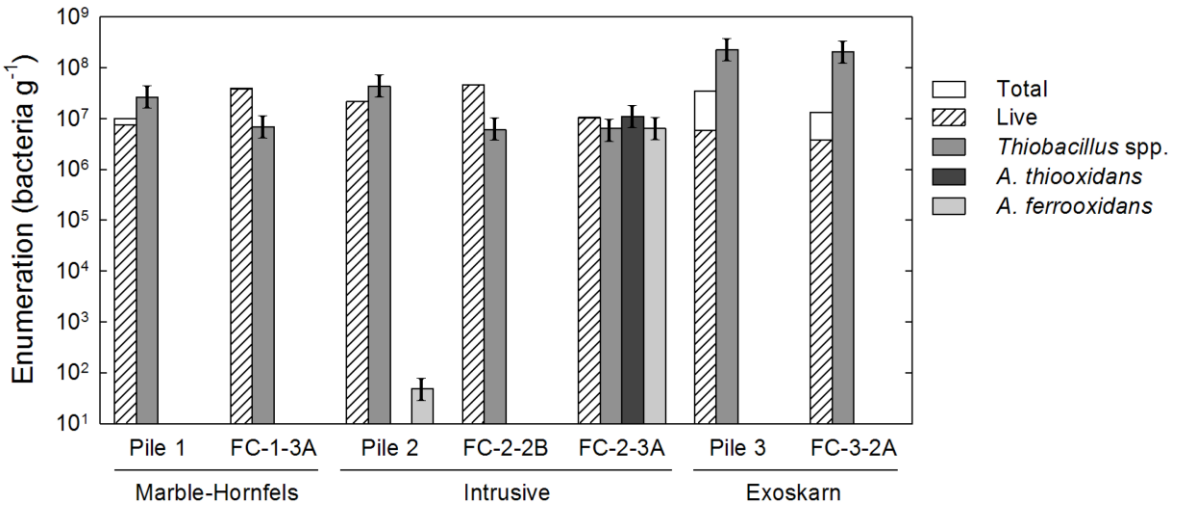

Fluorescent *in situ* hybridization (FISH) imaging of samples revealed the presence of bacterial cells that hybridized with the genus-specific probes for *Acidithiobacillus* sp. (Thio820) in four of the seven samples (Piles 2 and 3, FC-2-3A, and FC-3-2A). The highest proportion of cells stained with both Thio820 and DAPI were observed in samples from Pile 3. Three bacterial cell morphologies were observed; slightly curved rods, highly curved rods, and filamentous bacteria. The most abundant cell morphology was the slightly curved rod, which was commonly observed during FE-SEM-EDS and the Live/Dead Baclight™ microscopy. This bacterial morphology is characteristic of *Acidithiobacillus* sp. and was observed in samples from Pile 2 and FC-2-3A. Less abundant were highly curved rod-shaped bacteria similar in morphology to *Leptospirillum* spp. [26] observed in sample FC-2-3A. Filamentous bacteria were observed in samples FC-2-2B, FC-3-2A, FC-1-3A, and Pile 3 during Live/Dead Baclight™ procedure. These filamentous bacteria are similar to *Thermothrix thiopara*, which is capable of thiosulfate oxidation at circumneutral pH [27]. Filamentous bacteria were not observed during FE-SEM imaging.

Although waste rock from Pile 1 and FC-1-3A (marble-hornfels) had been subjected to the longest period of oxidation, colonization by acidophiles was not apparent from MPN enumerations. Electron microscopy (FE-SEM) revealed a fine-grained secondary precipitate had accumulated within Pile 1; however, bacterial cells were not observed. Cumulative sulfate mass discharges were lowest for the

marble-hornfels waste rock when comparing results among corresponding experiments. Although colonization by acidophiles was not observed, the presence of Zn and Cu in drainage from FC-1-3A is indicative of ferric leaching of sphalerite and chalcopyrite (Reactions (1)–(3)). Limited discharge of these metals from Pile 2 is attributed to secondary controls (*i.e.*, co-precipitation, sorption) on their mobility within the experimental waste rock piles. Despite the higher pyrite content of the exoskarn waste rock, microbial communities in samples from Pile 3 and FC-3-2A also were dominated by neutrophilic *Thiobacillus* spp. at similar populations to those observed for the marble-hornfels waste rock. Calcite comprised a smaller component of the exoskarn mineral assemblage compared to that of marble-hornfels; however, this waste rock type exhibited the highest pyrite content (Table 2). The presence of bacteria associated with a thin filamentous film at the grain margin suggests involvement in sulfide-mineral oxidation. However, limited biofilm development and a general lack of secondary Fe(III) precipitates suggests that growth on *A. ferrooxidans* or other acidophilic bacteria were pH limited. Drainage from the experiments containing exoskarn also exhibited circumneutral average pH values of 7.5 (Pile 3) and 7.3 (FC-3-2A). Nonetheless, cumulative mass discharges for sulfate and zinc were the highest compared among experimental piles or field cells. The relatively rapid colonization of intrusive waste rock type by acidophiles, combined with a general lack of acidophiles in marble-hornfels and exoskarn waste rock, indicate that carbonate-mineral content and bulk pH controlled the colonization of sulfide-minerals by acidophilic bacteria.

$$Fe^{2+} + H^{+} + ¼\ O_2 \rightarrow Fe^{3+} + ½\ H_2O;\ \text{biotic} \quad (1)$$

$$8\ Fe^{3+} + ZnS + 4\ H_2O \rightarrow 8\ Fe^{2+} + Zn^{2+} + SO_4^{2-} + 8\ H^{+};\ \text{abiotic} \quad (2)$$

$$14\ Fe^{3+} + FeCuS_2 + 7\ H_2O \rightarrow 15\ Fe^{2+} + Cu^{2+} + 2\ SO_4^{2-} + 14\ H^{+};\ \text{abiotic} \quad (3)$$

In addition to *Thiobacillus* spp., microbial communities within samples from Pile 2 and FC-2-3A (intrusive) included viable populations of acidophilic iron oxidizers. The largest population of acidophilic iron oxidizers was found in FC-2-3A, which also was characterized by an elevated population of acidophilic sulfur oxidizers and an average annual drainage pH of 6.2. These bacteria appear to have colonized the sulfide mineral surface initially by direct attachment, cementation and formation of an acidic expansion front (Pile 2; Figure 3), as proposed by Mielke *et al.* [18]. The extensive occurrence of microbially-colonized Fe(III) (oxy)hydroxysulfate, e.g., jarosite ($KFe_3(OH)_6(SO_4)_2$) and Fe(III) (oxy)hydroxide phases within FC-2-3A suggests that formation of these precipitates may support growth of acidophilic bacteria in NRD systems following the initial colonization stage (below). The occurrence of acidophiles in Pile 2 and FC-2-3A is attributed to the low calcite content of the intrusive waste rock, which may facilitate the rapid development of an acidic layer at sulfide-mineral surfaces. Cumulative mass discharges for sulfate were similar between intrusive and marble-hornfels waste rock for a given experiment (*i.e.*, experimental piles or field cells); however, precipitation of gypsum or other sulfate phases may complicate relative comparisons of sulfate discharge among waste rock types.

3.3. Mineralogy and X-ray Absorption Spectroscopy

Weathered sulfide minerals from the three waste rock piles, and one field cell FC-2-3A that exhibited elevated populations of acidophilic bacteria, were selected for detailed examination by FE-SEM-EDS.

Bacterial cells were generally sparse on samples from the field cells; however, surfaces of weathered pyrite grains from Pile 2 were colonized by bacteria (Figure 3A). For Pile 2, dissolution pits surrounded by secondary minerals were observed in the absence of bacterial cells at the surface of a chalcopyrite grain (Figure 3B). The occurrence of secondary precipitates surrounding the dissolution pit is indicative of bacterial attachment, which has been associated with localized precipitation of Fe(III) phases at cell margins and on EPS deposits [18,28,29]. Despite exhibiting the highest MPN population of neutrophilic thiosulfate oxidizers, relatively few bacterial cells were observed at chalcopyrite or pyrite surfaces in samples collected from Pile 3 (data not shown).

Figure 3. Field emission-scanning electron microscopy secondary electron (FE-SEM SE) micrographs of: (**A**) bacterially-colonized secondary Fe(III) (oxy)hydroxysulfate precipitates at the sulfide-mineral surface in FC-2-3A (EDS analysis indicated the presence of Fe, S and O—data not shown); and (**B**) relic direct attachment pits at the surface of a chalcophyrite grain in Pile 2. Scale bars equal 3 μm.

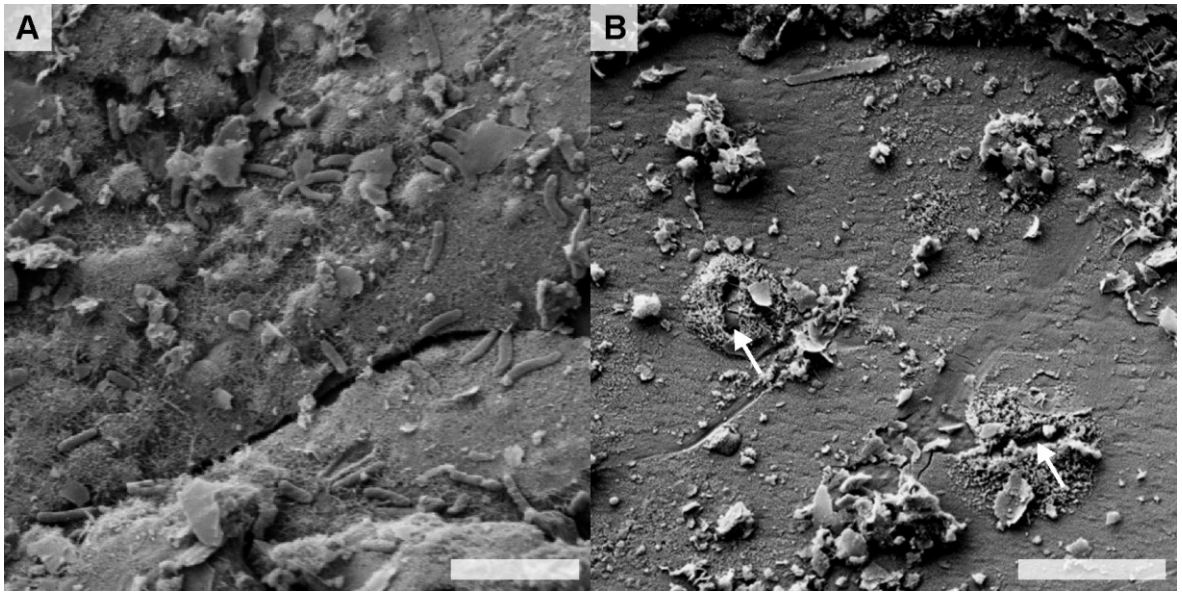

A macroscopic sulfide clast comprised of chalcopyrite, pyrrhotite, sphalerite and pyrite (based on EDS analyses), and characterized by the presence of extensive weathering products was selected from FC-2-3A for detailed analysis. Imaging of the weathered clast by FE-SEM revealed extensive secondary mineral-precipitation and biofilm formation at mineral surfaces. Bacterial cells were largely associated with porous precipitate localized at surfaces of weathered pyrite and pyrrhotite within the clast (Figures 4–6). The highest density of bacterial cells was observed within this porous layer rather than on the underlying mineral surfaces (Figure 4). This secondary-precipitate layer exhibited the fibrous morphology characteristic of schwertmannite, and was commonly bound between the sulfide-mineral surface and a less porous, smooth precipitate crust (Figure 4A). The mineralogical composition of this secondary Fe(III)-bearing coating could not be distinguished from primary phases in powder XRD analysis of liberated grains. However, LCF of bulk Fe K-edge EXAFS spectra (X^2 = 0.44) was achieved by fitting pyrite, schwertmannite [$Fe_8O_8(OH)_{6-4.5}(SO_4)_{1-1.75}$], lepidocrocite [γ-FeO(OH)] and K-jarosite [$KFe_3(OH)_6(SO_4)_2$] (Figure 5). The fitted ratio of schwertmannite to lepidocrocite to

K-jarosite was found to be 4.2:1.6:1, indicating that schwertmannite was the most abundant secondary Fe-bearing precipitate within the secondary mineral coating on this weathered sulfide grain. Pitting of the pyrrhotite surface was observed for a location where the schwertmannite had become detached, whereas pitting was limited to the adjacent pyrrhotite surface (Figure 4D). This observation suggests that the Fe incorporated into schwertmannite is derived from dissolution of the underlying sulfide-mineral surface.

Figure 4. FE-SEM SE micrographs of: (**A**) a exposed region of porous schwertmannite covered by a thin, non-porous crust; (**B**) bacteria within the porous schwertmannite layer observed at higher magnification; (**C**) bacterially-colonized porous schwertmannite beneath the thin, non-porous crust; and (**D**) an area of bacterially-colonized schwertmannite that separated from sulfide-mineral surface revealing extensive pitting. Scale bars equal 10 μm, 1 μm, 1 μm and 1 μm, respectively.

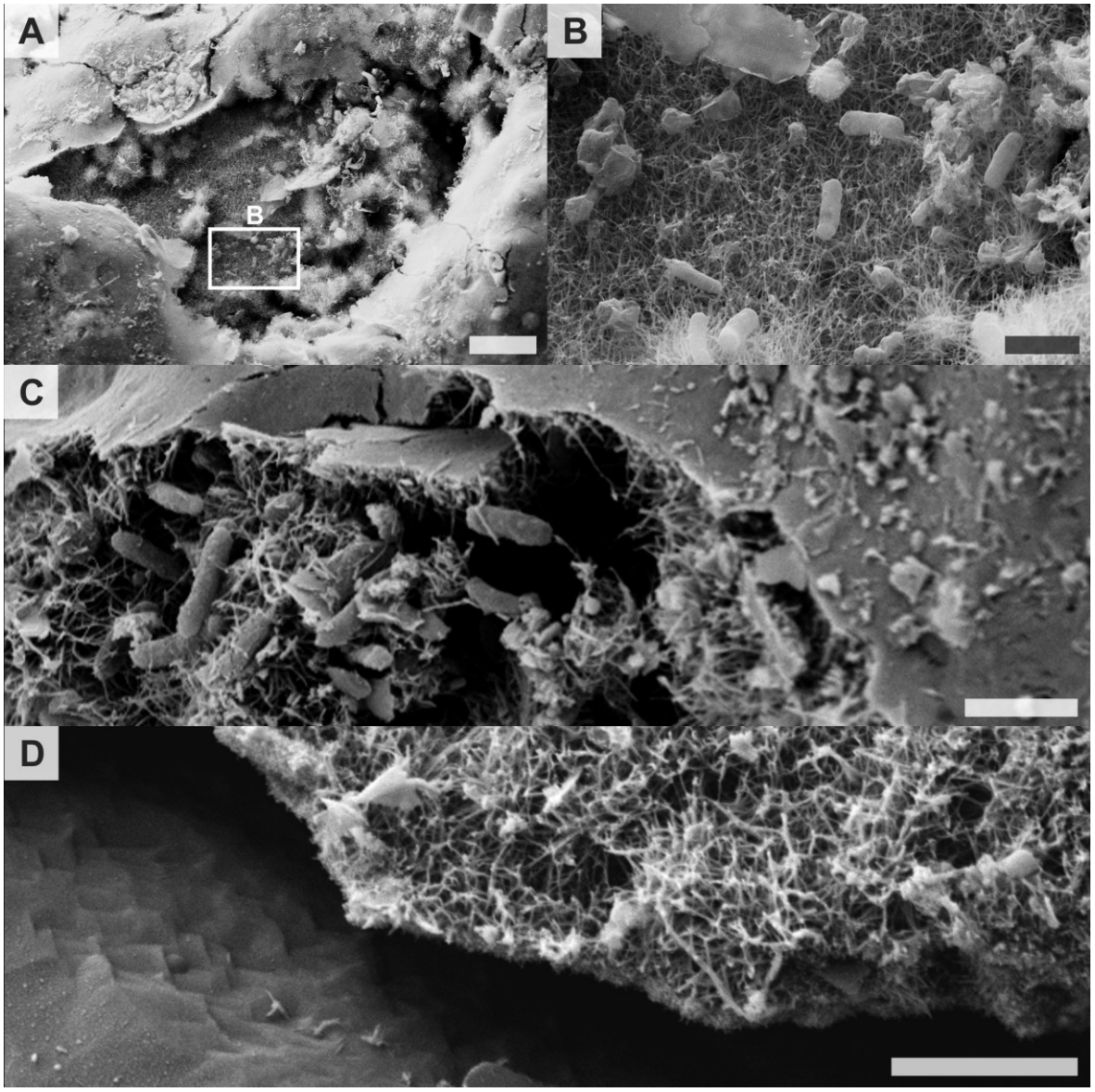

Figure 5. FE-SEM SE micrograph of microbially-colonized, secondary Fe-bearing mineral coating on surface of a sulfide-mineral clast from intrusive waste rock (FC-2-3A). Scale bar equals 5 μm. Corresponding bulk Fe K-edge extended X-ray absorption fine structure (EXAFS) spectra (solid line) and linear combination fitting (LCF) fit (circles) of sulfide-mineral weathering products.

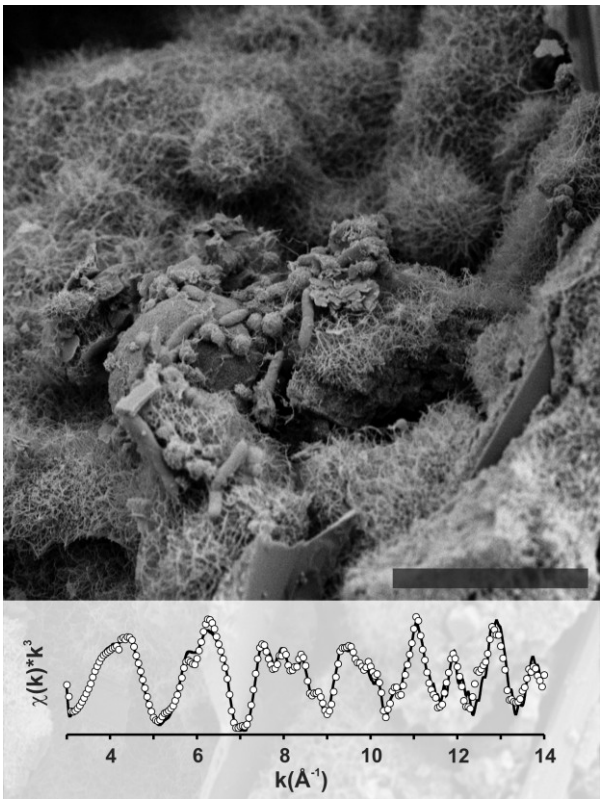

A transect measuring ~30 μm long was FIB milled through the schwertmannite-rich layer near an exposed pyrrhotite surface to facilitate FE-SEM-EDS examination across this layer (Figure 6). Three distinct layers exhibiting different chemical composition and texture were observed in SE images showing this cross-section (Figure 6D). The upper layer was composed of an Fe–S–O precipitate containing minor amounts of Si. The molar Fe:S ratio of this layer was 8:2.4, which is similar to the 8:(1–1.75) molar ratio that is characteristic of schwertmannite. Slight variation from the ideal molar ratio may result from the precipitation of sulfate phases during sample drying. A lighter-colored intermediate Fe–O–Si layer contained ~20% (molar) Si and trace concentrations of Al content. A distinct transition from the middle Fe–O–Si layer to a lighter colored Fe–O layer was observed, which was comprised solely of Fe and O. The porosity of the upper schwertmannite layer was estimated to be 8.2% based on two dimensional binary image analysis of the SE image. Approximately 50% of this porosity was associated with a large void located in the upper left quadrant of the image (Figure 6D,E). The porosity of the upper schwertmannite layer, which was poorly preserved during FIB milling, is likely much greater at zones more distal to the primary sulfide-mineral surface.

Poorly ordered ferrihydrite [nominally $Fe_2O_3 \cdot ½H_2O$] and schwertmannite generally are the first Fe(III) phases to precipitate during oxidation of iron-sulfide minerals [30,31]. These minerals are metastable with respect to more crystalline and less soluble Fe(III) (oxy)hydroxides, and will transform to goethite [αFeOOH] at circumneutral pH with lepidocrocite [γFeOOH] commonly forming

as an intermediate phase [30,32–35]. Under low-pH conditions (*i.e.*, pH ≤ 3), these Fe(III) (oxy)hydroxides can transform to jarosite in the presence of monovalent cations [30,36,37]. Due to the nano-crystalline nature schwertmannite, and the geochemical conditions under which this phase forms, schwertmannite has been commonly identified as the predominant Fe precipitate produced by acidophilic iron oxidizing bacteria [36,38–41]. Dissolved Fe concentration in drainage from the experimental piles and field cells generally remained below the method detection limit (0.001 $mg \cdot L^{-1}$) due to the low solubility of Fe(III) in circumneutral pH waters. This result precluded geochemical equilibrium modeling of associated mineral saturation indices.

Figure 6. FE-SEM SE micrographs of: (**A**) an overview of the surface of a bacterially-colonized, weathered pyrrhotite grain with areas selected for higher magnification imaging; (**B**) a bacterially-colonized layer of porous schwertmannite and adjacent pyrrhotite surface exhibiting no direct bacterial attachment; (**C**) a mineralised biofilm surrounded by porous schwertmannite with non-porous crust present at the top of the image; (**D**) three different layers of iron oxides exposed by the focused ion beam (FIB) cut; and (**E**) mineralized bacteria (arrows) within the micrometer-scale porous structure located approximately 5 µm below the outer margin of the schwertmannite layer. Scale bars equal 50 µm, 5 µm, 2 µm, 5 µm and 0.5 µm, respectively.

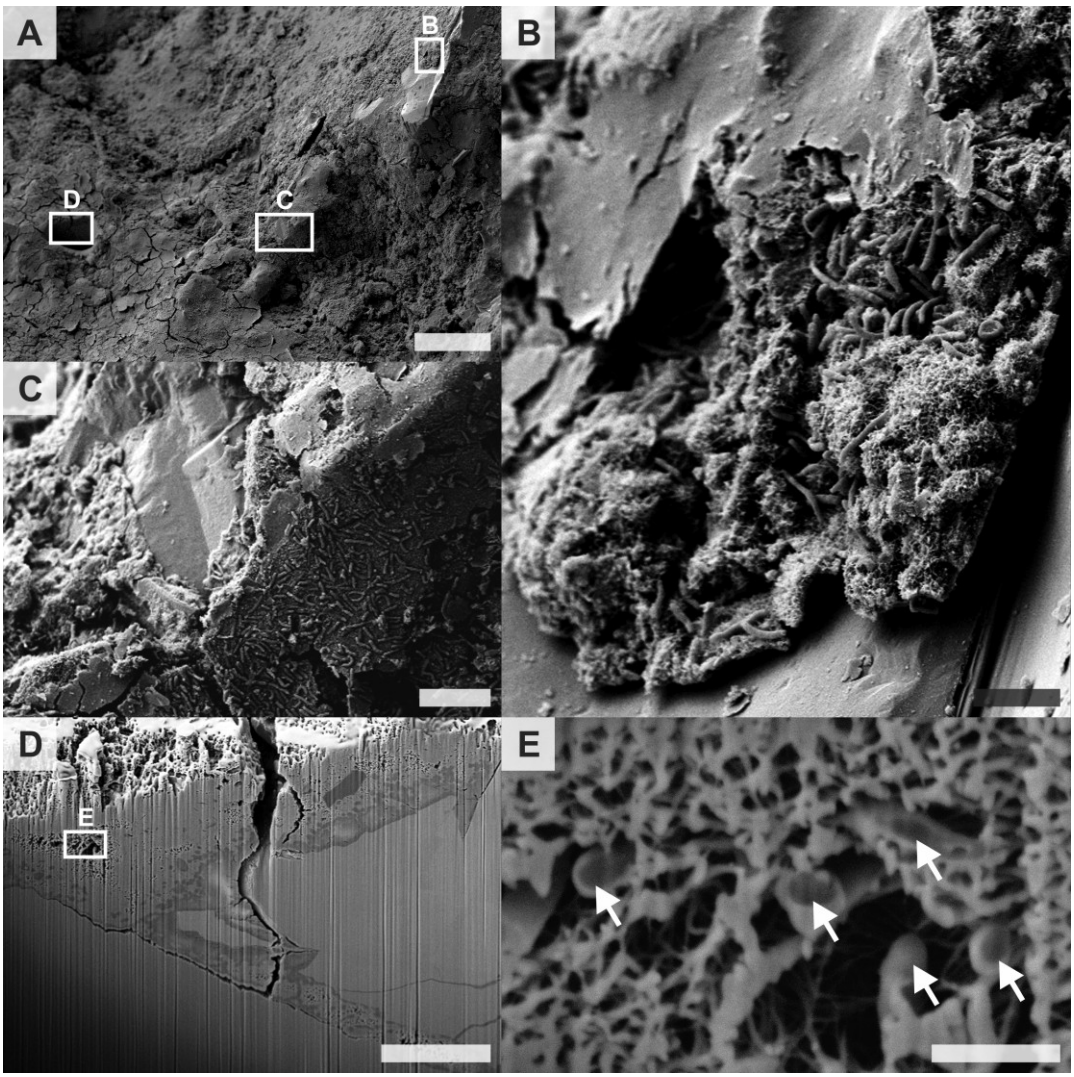

The biogeochemical conditions under which ferrihydrite or schwertmannite will precipitate remains somewhat uncertain [42]. Thermodynamic-based predictions indicate that ferrihydrite precipitation is favored at circumneutral and alkaline pH, whereas schwertmannite precipitation is favored under circumneutral to acidic pH conditions [33,37,38]. The average pH of drainage from FC-2-3A initially was mildly alkaline (pH > 8), but decreased to 6.2–6.5 after approximately 3 months. Under bulk circumneutral pH conditions observed in this field cell, the precipitation of schwertmannite may be thermodynamically favored in the presence of sulfate [42]. Iron K-edge EXAFS spectra indicated that schwertmannite was the dominant Fe-bearing precipitate on the weathered sulfide clast from FC-2-3A (intrusive), while lesser amounts of K-jarosite and lepidocrocite were present. Bigham *et al.* [33] found that schwertmannite was the predominant Fe(III) phase in acid sulfate waters (n = 28) at pH 2.8–4.5, whereas K-jarosite dominated at pH < 2.5 and mixtures of ferrihydrite and goethite occurred at pH > 6.5. The presence of both schwertmannite and K-jarosite on this weathered sulfide clast is indicative of the development of an acidic microenvironment at the sulfide mineral surface, *i.e.*, is an important habitat, in this intrusive waste rock (FC-2-3A), which at the time of sample collection was characterized by bulk NRD conditions.

3.4. Bacteria-Mineral Interactions

Examination of sulfides using FE-SEM revealed that bacteria in the FC-2-3A intrusive sample were commonly associated with schwertmannite at the weathered sulfide-mineral surface (Figures 3C and 4–6). These bacteria occurred within the porous structure of schwertmannite, which was often covered with a thin, non-porous crust (Figure 5A,C). Bacteria were also found in porous schwertmannite on the fringe of the crusted region (Figure 4C), and buried within schwertmannite between the crust and the sulfide mineral surface (Figure 6D,E). The crust formed only in regions with thick schwertmannite layers, suggesting that changes in biogeochemical conditions at greater distance from the sulfide-mineral surface may not favor schwertmannite precipitation. The abundance of bacteria within the porous schwertmannite layer indicates that precipitation of this mineral phase is an important microbial habitat. This layer has potential to provide isolation from bulk geochemical conditions within the waste rock, thereby facilitating the development of an acidic microenvironment.

Intuitively, the porosity within the schwertmannite must be amenable to microbial growth. Sulfide surfaces covered with the non-porous lower two layers exposed in the FIB transect (Figure 6D) demonstrate that sulfides may quickly become armored. However, the oxidation of sulfide minerals coated by porous schwertmannite may be subjected to ongoing oxidation due to the diffusive transport of oxidants through this layer. If sulfide mineral surfaces continue to be oxidized beneath the porous schwertmannite, acidic conditions could persist within the pore space of the schwertmannite. This mechanism was inferred where a schwertmannite layer became detached from the underlying pyrrhotite surface, exposing dissolution pitting uncharacteristic of bacterial attachment [18,19,28,43]. The occurrence of K-jarosite in FC-2-3A reflects the presence of acidic conditions at the sulfide-mineral surfaces, and indicates that Fe(III) contributes to sulfide-mineral oxidation in this NRD system.

The direct attachment model is often used to explain the colonization of acidophilic bacteria in circumneutral pH environments [18,44]. This model describes the development of acidic microenvironment at the bacteria-mineral interface, where increased Fe(III) solubility facilitates Fe

redox cycling coupled with sulfide oxidation [18]). Relic direct attachment sites (*i.e.*, pits) on the chalcopyrite surface in Pile 2 (Figure 2B) were surrounded by a secondary Fe(III) precipitate, presumably reflecting direct attachment by acidophiles. The secondary Fe(III) precipitate associated with the attachment sites exhibited a tubular structure similar to schwertmannite, which is in distinct contrast to precipitates not associated with attachment sites. Acidophilic iron oxidizing bacteria can promote the precipitation of Fe(III) (oxy)hydroxide and Fe(III) (oxy)hydroxysulfate minerals on or near the cell surface [29]). The close association of attachment sites and secondary Fe(III) precipitates, combined with limited pitting in surrounding areas of the chalcopyrite surface, suggest that acidophilic bacteria were facilitating sulfide-mineral oxidation via Fe(III) generation. Acidophilic iron oxidizing bacteria were not abundant, but viable populations were cultured from Pile 2 (intrusive), where these relic direct attachment sites were observed. The expansion of acidic microenvironments from initial attachment sites appears to have been facilitated through precipitation of schwertmannite and K-jarosite, which supported the larger populations of acidophilic bacteria observed in FC-2-3A.

3.5. Implications for Drainage Quality

Rates of sulfide-mineral oxidation are dependent on the activity of lithoautotrophic bacteria [10]. Hollings *et al.* [45] demonstrated that microbial activity accounted for a doubling of O_2 consumption rates—a proxy for sulfide-mineral oxidation—in sulfidic waste rock characterized by NRD conditions. At circumneutral pH, the chemical oxidation of sulfide-minerals by Fe(III) could be expected to be limited by the low solubility of this electron acceptor. However, development of acidic microenvironments at sulfide-mineral surfaces may support localized increases in Fe(III) solubility and sulfide-mineral oxidation rates. Rates of abiotic Fe(II) oxidation are relatively slow at pH < 4, making this process a potential rate-limiting step in in the oxidation of sulfide minerals [8,9]. However, the microbial catalysis of Fe(II) oxidation can greatly increase rates of Fe(III) generation, and therefore sulfide-mineral oxidation, under acidic conditions [10].

The relative increase in MPN populations of acidophilic iron and sulfur oxidizers within intrusive waste rock (FC-2-3A) is indicative of a transition in the microbial community towards ARD conditions. This transition has previously been observed prior to acidification of mine waste [1,12,44]. Although bulk drainage pH for this waste rock remained circumneutral during the study period, a transition from NRD to ARD conditions would result in substantial changes in drainage chemistry. Dissolved concentrations of several metals (*i.e.*, Fe, Zn, Cu) generally exhibit an indirect relationship with pH; therefore, the development of ARD conditions would have important implications for water quality management.

4. Conclusions

Results of this study indicate that extensive development of acidic microenvironments may support growth of acidophilic bacteria within bulk neutral rock drainage settings. The formation of porous schwertmannite layers at sulfide-mineral surfaces supported relatively large populations of acidophilic bacteria, which likely were contributing to sulfide-mineral oxidation by generating Fe(III) for sulfide-mineral oxidation. Assuming bulk pore-water chemistry is amenable to schwertmannite stability, the ongoing growth of this schwertmannite layer is expected to facilitate proliferation of

acidophilic iron oxidizing bacteria. A principal implication of the development of this acidic microenvironment is the potential for increased oxidation rates due to localized increases in Fe(III) solubility at sulfide-mineral surfaces. Limited growth of acidophiles in waste rock characterized by higher calcite contents (*i.e.*, marble-hornfels, exoskarn) indicates that the formation of acidic microenvironments is inhibited or delayed by carbonate dissolution reactions.

Waste rock environments are highly heterogeneous with respect to both mineralogy and geochemistry [46]. Although the field cell containing intrusive waste rock (FC-2-3A) exhibited varied microbial and geochemical characteristics to the other experiments, this system provided the ideal opportunity to evaluate processes controlling the transition from circumneutral to acidic pH conditions. Geochemical conditions favorable to extensive growth of acidophilic bacteria clearly can develop within mine wastes characterized by bulk circumneutral pH drainage. This information is critical for the development of innovative strategies for managing water quality in neutral rock drainage settings.

Acknowledgments

We thank Celedonio Aranda, Sharon Blackmore, Stephane Brienne, Bevin Harrison, Trevor Hirsche and Holly Peterson for logistical and technical contributions. We also thank Dr. Ben Kocar of Stanford University for performing XAS analysis. Funding was provided by Compañía Minera Antamina S.A., Teck Resource Ltd., and the Natural Sciences and Engineering Research Council of Canada (NSERC) through a Collaborative Research and Development (CRD) grant and through the NSERC Discovery program (Southam).

Author Contributions

Mayer and Beckie had the original concept for the project. Southam provided guidance on linking microbiology to geochemistry and mineralogy. Dockrey and Lindsay were a MSc and post-doctoral fellow at UBC who worked on the project and produced the first draft of the manuscript; both visited Southam's laboratory. Norlund and Warren provided their molecular expertise to the bacterial identifications. All authors were involved with data interpretation and in writing the manuscript.

Conflicts of Interest

The authors declare no conflict of interest.

References

1. Blowes, D.W.; Ptacek, C.J.; Jambor, J.L.; Weisener, C.G. The geochemistry of acid mine drainage. *Treatise Geochem.* **2003**, *9*, 149–204.
2. Nordstrom, D.K. Hydrogeochemical processes governing the origin, transport and fate of major and trace elements from mine wastes and mineralized rock to surface waters. *Appl. Geochem*. **2011**, *26*, 1777–1791.
3. Jurjovec, J.; Ptacek, C.J.; Blowes, D.W. Acid neutralization mechanisms and metal release in mine tailings: A laboratory column experiment. *Geochim. Cosmochim. Acta* **2002**, *66*, 1511–1523.

4. Heikkinen, P.M.; Räisänen, M.L.; Johnson, R.H. Geochemical characterisation of seepage and drainage water quality from two sulphide mine tailings impoundments: Acid mine drainage *versus* neutral mine drainage. *Mine Water Environ*. **2009**, *28*, 30–49.
5. Lindsay, M.B.J.; Condon, P.D.; Jambor, J.L.; Lear, K.G.; Blowes, D.W.; Ptacek, C.J. Mineralogical, geochemical, and microbial investigation of a sulfide-rich tailings deposit characterized by neutral drainage. *Appl. Geochem*. **2009**, *24*, 2212–2221.
6. Nordstrom, D.K.; Alpers, C.N.; Ptacek, C.J.; Blowes, D.W. Negative pH and extremely acidic mine waters from Iron Mountain, California. *Environ. Sci. Technol*. **2000**, *34*, 254–258.
7. Moncur, M.C.; Ptacek, C.J.; Blowes, D.W.; Jambor, J.L. Release, transport and attenuation of metals from an old tailings impoundment. *Appl. Geochem*. **2005**, *20*, 639–659.
8. Singer, P.C.; Stumm, W. Acidic mine drainage: The rate determining step. *Science* **1970**, *167*, 1121–1123.
9. Williamson, M.A.; Rimstidt, J.D. The kinetics and electrochemical rate-determining step of aqueous pyrite oxidation. *Geochim. Cosmochim. Acta* **1994**, *58*, 5443–5454.
10. Nordstrom, D.K.; Southam, G. Geomicrobiology of sulfide mineral oxidation. *Rev. Mineral*. **1997**, *35*, 361–390.
11. Southam, G.; Beveridge, T.J. Enumeration of thiobacilli within pH-neutral and acidic mine tailings and their role in the development of secondary mineral soil. *Appl. Environ. Microbiol*. **1992**, *58*, 1904–1912.
12. Blowes, D.W.; Al, T.A.; Lortie, L.; Gould, W.D.; Jambor, J.L. Microbiological, chemical and mineralogical characterization of the Kidd Creek Mine Tailings Impoundment, Timmins area, Ontario. *Geomicrobiol. J*. **1995**, *13*, 13–31.
13. Blowes, D.W.; Jambor, J.L.; Hanton-Fong, C.J.; Lortie, L.; Gould, W.D. Geochemical, mineralogical and microbiological characterization of a sulphide-bearing carbonate-rich gold mine tailings impoundment, Joutel, Quebec. *Appl. Geochem*. **1998**, *13*, 687–705.
14. Goldhaber, M.B. Experimental study of metastable sulfur oxyanion formation during pyrite oxidation at pH 6–9 and 30 °C. *Amer. J. Sci*. **1983**, *283*, 193–217.
15. Moses, C.O.; Herman, J.S. Pyrite oxidation at circumneutral pH. *Geochim. Cosmochim. Acta* **1991**, *55*, 471–482.
16. Schippers, A.; Jozsa, P.-G.; Sand, W. Sulfur chemistry in bacterial leaching of pyrite. *Appl. Environ. Microbiol*. **1996**, *62*, 3424–3431.
17. Dopson, M.; Lindstrom, E.B. Potential role of *Thiobacillus caldus* in arsenopyrite bioleaching. *Appl. Environ. Microbiol*. **1999**, *65*, 36–40.
18. Mielke, R.E.; Pace, D.L.; Porter, T.; Southam, G. A critical stage in the formation of acid mine drainage: Colonization of pyrite by *Acidithiobacillus ferrooxidans* under pH-neutral conditions. *Geobiology* **2003**, *1*, 81–90.
19. Pace, D.L.; Mielke, R.E.; Southam, G.; Porter, T.L. Scanning force microscopy studies of the colonization and growth of *A. ferrooxidans* on the surface of pyrite minerals. *Scanning* **2005**, *27*, 136–140.
20. Sand, W.; Gehrke, T.; Hallman, R.; Schippers, A. Sulfur chemistry, biofilm, and the (in)direct attack mechanism—A critical evaluation of bacterial leaching. *Appl. Microbiol. Biotechnol*. **1995**, *43*, 961–966.

21. Love, D.A.; Clark, A.H. The lithologic, stratigraphic, and structural setting of the giant Antamina copper-zinc skarn deposit, Ancash, Peru. *Econ. Geol.* **2004**, *99*, 887–916.
22. Webb, S.M. SIXpack: A graphical user interface for XAS analysis using IFEFFIT. *Phys. Scr.* **2005**, *2005*, 1011–1014.
23. Strömberg, B.; Banwart, S.A. Experimental study of acidity-consuming processes in mining waste rock: some influences of mineralogy and particle size. *Appl. Geochem*. **1999**, *14*, 1–16.
24. Cochran, W.G. Estimation of bacterial densities by means of the "most probable number". *Biometrics* **1950**, *6*, 105–116.
25. Amann, R.I.; Ludwig, W.; Schleifer, K.H. Phylogenetic identification and *in situ* detection of individual microbial cells without cultivation. *Microbiol. Rev*. **1995**, *59*, 143–169.
26. Chapana, R.J.A.; Tributsch, H. Interfacial activity and leaching patterns of *Leptospirillum ferrooxidans* on pyrite. *FEMS Microbiol. Ecol*. **2004**, *47*, 19–29.
27. Brannan, L.D.K.; Caldwell, D.E. *Thermothris thiopara*: Growth and metabolism of a newly isolated thermophile capable of oxidizing sulfur and sulfur compounds. *Appl. Environ. Microbiol*. **1980**, *40*, 211–216.
28. Edwards, K.J.; Hu, B.; Hamers, R.J.; Banfield, J.F. A new look at microbial leaching patterns on sulfide minerals. *FEMS Microbiol. Ecol*. **2001**, *34*, 197–206.
29. Fortin D.; Langley, S. Formation and occurrence of biogenic iron-rich minerals. *Earth Sci. Rev.* **2005**, *72*, 1–19.
30. Jang, J.H.; Dempsey, B.A.; Catchen, G.L.; Burgos, W.D. Effects of Zn(II), Cu(II), Mn(II), Fe(II), NO_3^-, or SO_4^{2-} at pH 6.5 and 8.5 on transformation of hydrous ferric oxide (HFO) as evidenced by Mössbauer spectroscopy. *Colloids Surf. A* **2003**, *22*, 55–68.
31. Regenspurg, S.; Brand, A.; Peiffer, S. Formation and stability of schwertmannite in acidic mining lakes. *Geochim. Cosmochim. Acta* **2004**, *68*, 1185–1197.
32. Schwertmann, U.; Taylor, R.M. The influence of silicate on the transformation of lepidocrocite to goethite. *Clays Clay Miner*. **1972**, *20*, 159–164.
33. Bigham, J.M.; Schwertmann, U.; Traina, S.J.; Winland, R.L.; Wolf, M. Schwertmannite and the chemical modeling of iron in acid sulfate waters. *Geochim. Cosmochim. Acta* **1996**, *60*, 2111–2121.
34. Jönsson, J.; Persson, P.; Sjöberg, S.; Lövgren, L. Schwertmannite precipitated from acid mine drainage: Phase transformation sulphate release and surface properties. *Appl. Geochem*. **2005**, *20*, 179–191.
35. Schwertmann, U.; Carlson, L. The pH dependent transformation of schwertmannite to goethite at 25 °C. *Clay Miner*. **2005**, *40*, 63–66.
36. Schwertmann, U.; Bigham J.M.; Murad, E. The first occurrence of schwertmannite in a natural stream environment. *Eur. J. Miner*. **1995**, *7*, 546–552.
37. Yu, J.Y.; Heo, B.; Choi, I.K.; Cho, J.P.; Chang, H.W. Apparent solubilities of schwertmannite and ferrihydrite in natural stream waters polluted by mine drainage. *Geochim. Cosmochim. Acta* **1999**, *63*, 3407–3416.
38. Kawano, M.; Tomita, K. Geochemical modeling of bacterially induced mineralization of schwertmannite and jarosite in sulfuric acid spring water. *Am. Miner*. **2001**, *86*, 1156–1165.
39. Fukushi, K.; Sasaki, M.; Sato, T.; Yanase, N.; Amano, H.; Ikeda, H. A natural attenuation of arsenic in drainage from an abandoned arsenic mine dump. *Appl. Geochem*. **2003**, *18*, 1267–1278.

40. Liao, Y.; Zhou, L.; Liang, J.; Xiong, H. Biosynthesis of schwertmannite by *Acidithiobacillus ferrooxidans* cell suspensions under different pH condition. *Mater. Sci. Eng. C* **2009**, *29*, 211–215.
41. Liao, Y.; Zhou, L.; Bai, S.; Liang, J.; Want, S. Occurrence of biogenic schwertmannite in sludge bioleaching environments and its adverse effect on solubilization of sludge-borne metals. *Appl. Geochem*. **2009**, *24*, 1739–1746.
42. Majzlan, J.; Navrotsky, A.; Schwertmann, U. Thermodynamics of iron oxides: Part III. Enthalpies of formation and stability of ferrihydrite ($Fe(OH)_3$), schwertmannite ($FeO(OH)_{3/4}(SO_4)_{1/8}$) and ε-$Fe_2O_3$. *Geochim. Cosmochim. Acta* **2004**, *68*, 1049–1059.
43. Pisapia, C.; Humbert, B.; Chaussidon, M.; Mustin, C. Perforative corrosion of pyrite enhanced by direct attachment of *Acidithiobacillus ferrooxidans*. *Geomicrobiol. J*. **2008**, *25*, 261–273.
44. Southam, G.; Beveridge, T.J. Examination of lipopolysaccharide (O-Antigen) populations of *Thiobacillus ferrooxidans* from two mine tailings. *Appl. Environ. Microbiol*. **1993**, *59*, 1283–1288.
45. Hollings, P.; Hendry, M.J.; Nicholson, R.V.; Kirkland, R.A. Quantification of oxygen consumption and sulphate release rates for waste rock piles using kinetic cells: Cluff lake uranium mine, northern Saskatchewan, Canada. *Appl. Geochem*. **2001**, *16*, 1215–1230.
46. Nichol, C.; Smith, L.; Beckie, R. Field-scale experiments of unsaturated flow and solute transport in a heterogeneous porous medium. *Water Resour. Res*. **2005**, *41*, 1–11.

© 2014 by the authors; licensee MDPI, Basel, Switzerland. This article is an open access article distributed under the terms and conditions of the Creative Commons Attribution license (http://creativecommons.org/licenses/by/3.0/).